2015

Development of a Steerable Single-Actuator Cruciform Parachute

Fields, Travis D.; Yakimenko, Oleg A.

AIAA

Johnson, Bonnie, et al. "Complex Adaptive Systems of Systems: A Grounded Theory Approach." Grounded Theory Review 17.1 (2018).
http://hdl.handle.net/10945/71317

JOURNAL OF AIRCRAFT
Vol. 55, No. 3, May–June 2018

Development of a Steerable Single-Actuator Cruciform Parachute

Travis D. Fields*
University of Missouri–Kansas City, Kansas City, Missouri 64110
and
Oleg A. Yakimenko†
Naval Postgraduate School, Monterey, California 93943

DOI: 10.2514/1.C034416

Despite success in developing and fielding a family of different-weight precision self-guiding parafoil-based aerial payload delivery systems, there is a need for a system that would trade relatively large standoff deployment distances for a substantially lower cost of production and operation. One such system, based on a standard round canopy with a slightly modified rigging, was developed and demonstrated in the early 2000s. This paper capitalizes on controllable round canopy developments and considers using inexpensive cruciform-type canopies with a single-actuator control paradigm. Although the aerodynamics of cruciform-type canopies were extensively studied in the past, lesser efforts were devoted to converting them into a steerable platform. This paper presents the conceptual design and prototyping of a cruciform parachute-based aerial payload delivery system and discusses the results of the initial subscale developmental tests devoted to studying the control authorities and dynamics of such a system.

Nomenclature

$\mathcal{AR}$	=	canopy aspect ratio
C_D	=	canopy drag coefficient
GR	=	canopy glide ratio
K_D	=	derivative controller gain for the yaw angle proportional-integral-derivative controller, s
K_I	=	integral controller gain for the yaw angle proportional-integral-derivative controller, 1/s
K_P	=	proportional controller gain for the yaw angle proportional-integral-derivative controller
k	=	canopy asymmetry coefficient, 1/s
L	=	canopy arm length, m
l	=	suspension line length, m
l_c	=	length of the control suspension line(s), m
l_s	=	length of the static suspension line(s), m
S_0	=	area of the canopy material, m^2
V_d	=	canopy/payload descent velocity relative to atmospheric wind, m/s
V_G	=	vehicle ground speed, m/s
V_h	=	difference in ground speed between two parachute systems, m/s
W	=	canopy arm width, m
w_x, w_y, w_z	=	atmospheric wind velocity components, m/s
x, y, z	=	inertial coordinates in the local tangent north–east–down plane, m
δ_c	=	deflection of the control suspension line(s), m
δ_s	=	deflection of the static suspension line(s), m
ψ	=	canopy yaw angle about the canopy-fixed vertical axis, rad

I. Introduction

PRECISION aerial delivery operations have enabled significant humanitarian and military resupply efforts in scenarios where typical ground and air delivery operations are unsafe or infeasible. Several self-guided aerial delivery approaches have been developed over the past 20 years, with each seeking to provide a low-cost, minimally complex, and accurate precision delivery system [1].

Ram-air parafoils have been developed and integrated into current precision aerial delivery operations in both humanitarian and combat scenarios [1,2]. Ram-air parafoils are relatively inefficient air-filled gliding wings that can be controlled primarily in the lateral direction [1–4]. Small-scale parafoils have experimentally demonstrated very high landing location accuracy through the use of sophisticated path-planning and flight control algorithms [1,5]. Typical cargo parafoil glide ratios vary between 2:1 to 4:1, depending on the canopy geometry and incidence angle [1,6]. High-glide ratio systems enable large standoff distances; however, low-glide systems outperform the high-glide counterparts in terms of touchdown accuracy and maneuverability in highly congested environments. The U.S. Army Natick Soldier Research Development and Engineering Center (NSRDEC) began an investigation of using upper-surface spoilers, which were first investigated for glideslope control in the 1970s [7], for fully autonomously guided airdrop systems in 2010. A 0.96 m^2 small-scale ram-air canopy was recently modified to incorporate upper-surface spoilers in an attempt to create a variable glide ratio delivery system [8]. The lowest glide ratio occurs at the highest symmetric spoiler deflection, which corresponds with the highest vehicle descent rate.

As an alternative to ram-air parafoils, circular canopy control techniques were developed for traditional (inexpensive) round parachutes in which the circular canopy was either symmetrically or asymmetrically deformed. Symmetric deformation (reefing–disreefing) enables descent rate control, but it requires accurate knowledge of the winds to reach the desired landing location [9]. Fixed symmetric canopy deformation permits navigation toward a line segment (e.g., road), and it has been shown through simulation to provide increased landing location accuracy when compared to an uncontrolled delivery system [9]. A two-axis lateral guidance strategy was developed, enabling the delivery system to navigate toward a desired point location [10]. Experimental testing has been conducted to evaluate the various approaches to symmetrically deforming the canopy. Suspension line reefing provided high descent rate control, but it required a prohibitively large actuator for full-scale systems [11]. Control line reefing techniques have been evaluated for reversible reefing applications, and they have demonstrated high controllability with minimal actuator power requirements [12]. Regardless of the reefing technique used for descent rate control, the major limitation of symmetric deformation navigation is the lack of lateral control in the presence of no wind or wind prevailing in the wrong direction. Descent rate control can only reduce the wind drift error. It cannot directly counteract the wind because the vehicle is translated laterally, solely by

Presented as Paper 2017-3540 at the AIAA Aerodynamic Decelerator Systems Technology Conference, Denver, CO, 5–9 June 2017; received 13 February 2017; revision received 28 August 2017; accepted for publication 13 September 2017; published online 25 October 2017.

*Assistant Professor, Civil and Mechanical Engineering, 5110 Rockhill Rd., FH 352; fieldstd@umkc.edu. Senior Member AIAA.

†Professor, Department of Systems Engineering, Code SE/Yk; oayakime@nps.edu. Associate Fellow AIAA.

the prevailing winds. Asymmetric canopy deformation provides rudimentary lateral control authority (glide ratio of up to 0.8:1) by deflecting one or two of the four suspension line bridles [13]. Although the technique is capable of achieving some horizontal glide, the asymmetric deformation technique requires at least two large pneumatic [14,15] or large electromechanical actuators [16,17].

This paper incorporates the simplicity and low-cost aspects of the symmetric deformation approaches with the horizontal glide capabilities of the asymmetric deformation techniques applied to the inexpensive cruciform-type canopy. These canopies are composed of two identical fabric rectangles, which are crossed and joined to each other at the square intersection to form a flat surface having four equal arms. They were extensively studied in the past from the standpoint of structural integrity [18] and the effects of canopy geometry [19], including intentionally introduced asymmetry [20]. Potvin et al. performed an extensive field-testing regimen to explore the potential gliding capabilities of cruciform and hybrid cruciform canopies [21]. Their research yielded glide ratios of approximately 0.5 and 0.75 for cross and hybrid cruciform canopies with two added triangular panels (hycross), respectively. The research presented herein continues the development of Potvin et al. by implementing an onboard control system rather than the extensive flight testing conducted with fixed suspension lines.

The paper describes the initial testing of a novel control scheme that only requires one actuator and is organized as follows. Section II presents the conceptual framework for controlling a cruciform parachute using only a single actuator. Section III describes the small-scale hardware system that was developed. Section IV describes the experimental testing methodology designed for subscale testing of the aerial payload delivery system, followed by the Sec. V discussion of the flight-test results. Finally, Sec. VI concludes the single actuator-based aerial delivery system.

II. Concept of a Single-Actuator Control of a Cruciform Parachute

Nonsteerable cross-type canopies were introduced by Forichon in 1961 (Fig. 1a) [22]. Due to their simple design, good drag-to-canopy-area ratio, and good static and dynamic stability characteristics, they have been widely used in a variety of applications, including aircraft braking and decelerating other vehicles at the ground level, stabilization and deceleration of weapons, and recovery of high-altitude probe equipment. In its original design, the suspension lines of an equal length were attached to the outer edges of the four arms. For better performance, Forichon suggested using tie cords between the corners of the adjacent arms (the points D-E, F-A, B-G, and H-C in Fig. 1a), as shown in Fig. 1b. Many follow-up designs took advantage of the suggested improvement (Fig. 1c).

The three basic characteristics of cruciform-type parachute canopies are the arm length L, the arm width W, and the suspension line length l (Fig. 2). The aerodynamic effects of changing the ratio of

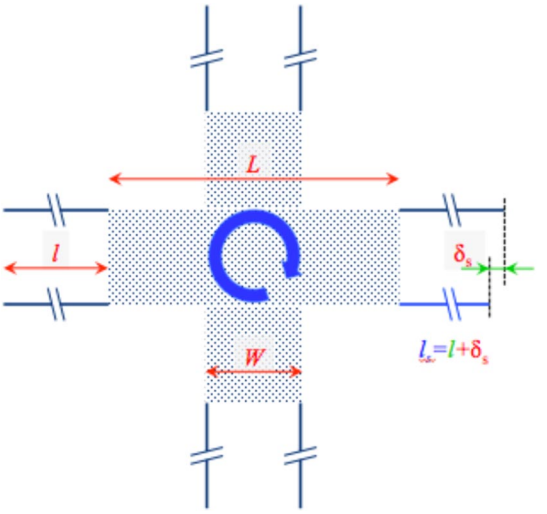

Fig. 2 Specifications of a cruciform parachute.

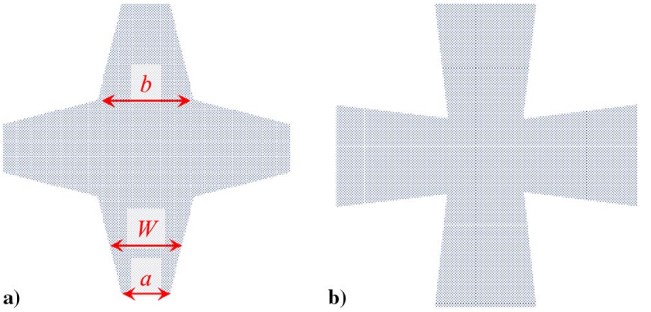

Fig. 3 Modifications of geometry of cross-type parachutes [19].

the arm length L and arm width W (within the 2.4 to 4 range), changing the ratio of the suspension line length l and arm length L (within 0.67 to 2), and varying cloth porosity and arm shape [i.e., the ratio of trapezoidal-shape arms a to b in Fig. 3 (within 0.5 to 2)] have been well studied [20,23–27].

Symmetrically designed cross-type parachutes have a tendency to rotate during descent. This asymmetry-driven rotation is caused by manufacturing inaccuracy, payload-induced asymmetry, initial deployment conditions, and the spin damping of the canopy. However, the methodology described herein uses asymmetric deformation to generate rudimentary glide. To fully capitalize the precision delivery capabilities of the system, the spin rate must be accurately controlled. Spin control can be achieved by intentionally introducing a difference in suspension

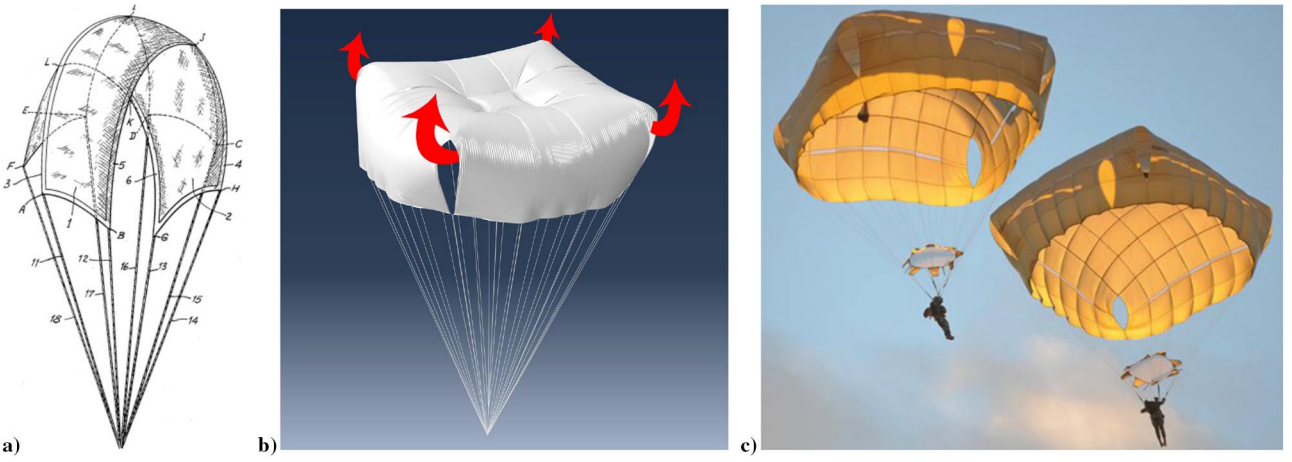

Fig. 1 Forichon's cross canopy, a tied-corners canopy design, and a fielded T-11 troop parachute.

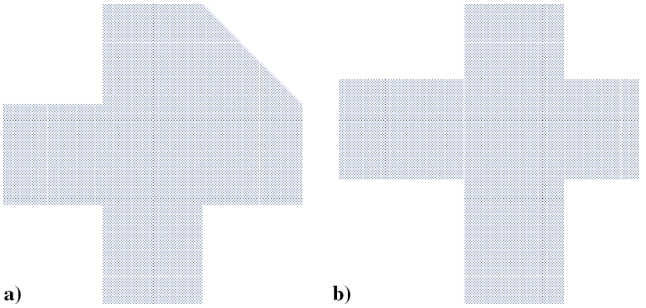

Fig. 4 Examples of asymmetric cross-type parachutes.

line lengths: $\delta_s - \delta_c$. Specifically, shortening one of the lines in a situation shown in Fig. 2 (featuring a top view) will result in clockwise (positive) spin.

In addition to spin rate controllability, the delivery system must be capable of rudimentary variable glide in order to be a viable precision delivery system. Gliding is achieved by modifying the cruciform-type parachute geometry and/or retrimming selected suspension lines (shortening or even removing certain suspension lines). For example, Fig. 4a features a canopy built out of a cruciform parachute and incorporating one triangular panel, the hycross parachute of Fig. 4b employs two shifted panels [21]. Potvin et al. [21] conducted the first field study assessing the effect of different retrimming the schemes on gliding capabilities and the spin rate by performing drop testing with a variety of static suspension line lengths in a myriad of configurations.

In this study, we address the problem of creating a glide capability while still using the standard symmetrically sewn cross canopy (Fig. 5).

The conceptual approach used to manipulate the gliding capabilities of the cross canopy entails creating an asymmetric deformation in the canopy geometry through a statically deformed suspension line and an adjacent servoactuated suspension line. One corner of a canopy panel (suspension line S in Fig. 5) is altered relative to the nominal suspension line length (change in line length of δ_s) and is fixed for the entire descent. From field testing, shortening the static line(s) creates a more stable canopy shape. Only results from static line lengths shorter than the nominal case ($\delta_s < 0$) are presented in this paper. In practice, the static line(s) could be fixed during the manufacturing process; however, in this study, a single suspension line was shortened manually before testing. With the static line shortened (and all other suspension line lengths equal to the nominal length), the canopy panel will curve downward more than the other three panels, thereby inducing a spin about the canopy-fixed vertical axis.

With the canopy in a spin, it produces negligible horizontal glide. The adjacent suspension line on the neighboring canopy panel can then be controlled with a servoactuator (labeled C in Fig. 5). If the controlled suspension line, coined the control line, is shortened the same amount as the static line deflection of $\delta_c = \delta_s$, the spin motion will cease. With two adjacent canopy panels deflected downward, the corresponding asymmetric deformation will create a rudimentary horizontal gliding motion. If the control line is further deflected downward ($\delta_c < \delta_s < 0$), the canopy will spin the opposite direction (counterclockwise for the configuration shown in Fig. 5).

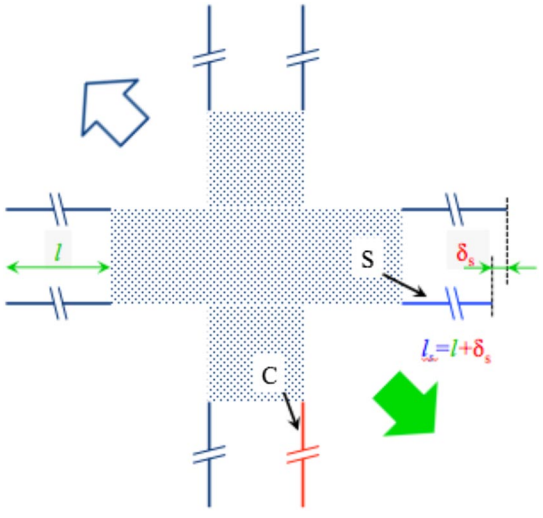

Fig. 5 Top-view layout of a controlled cruciform parachute.

The yaw rate motion can be expressed as a function of the static and control line lengths. The amount of suspension line deflection can be represented as $\delta_s = l_s - l$ and $\delta_c = l_c - l$ for the static and control lines, respectively. A $\delta_s < 0$ indicates a static line length that is shorter than the nominal suspension line length. A simple model for the spin rate is then determined by the difference between the static and control suspension line lengths as

$$\dot{\psi} = k(\delta_s)(\delta_s - \delta_c) \tag{1}$$

where $\dot{\psi}$ is the yaw rate in the parachute-fixed vertical axis, and $k(\delta_s)$ is an asymmetry coefficient that varies with the static line deflection (i.e., a greater static line deflection will exhibit a greater spin rate with zero control line deflection). A more complex second-order model may provide better accuracy, and both model structures are investigated further in Sec. V. For this feasibility study, a four-degree-of-freedom model is used to describe the dynamics of the system. Specifically, the relative motion between the parachute and payload, as well as the pitch and roll of the system, is neglected. Although these aspects will surely induce additional complexities in the modeling structure, the effects do not hinder the exploration of the conceptual framework as a precision delivery system.

The yaw rate $\dot{\psi}$ and static line deflection δ_s could directly affect the descent speed of the parachute as the vehicle is deformed (thereby reducing the effective drag area). Superimposed with the vertical wind speed component, the vertical motion can be described as

$$\dot{z} = V_d(\delta_s, \dot{\psi}) + w_z \tag{2}$$

where z is the vertical inertial coordinate in the local tangent north–east–down plane, $V_d(\delta_s, \dot{\psi})$ is the static line deflection and yaw-rate-dependent descent speed, and W_Z is the vertical wind speed component.

Finally, the horizontal translation of the parachute-payload system can be described with the glide ratio, which depends on the static line deflection and the yaw rate. As a conceptual example, the system will achieve maximum glide when the yaw rate is zero ($\delta_s = \delta_c$) and the glide ratio will be zero when the yaw rate is maximum. Combining with the atmospheric wind conditions, the horizontal translational kinematics are

$$\dot{x} = V_d(\delta_s, \dot{\psi}) GR(\delta_s, \dot{\psi}) \sin(\psi) + w_x \tag{3}$$

$$\dot{y} = V_d(\delta_s, \dot{\psi}) GR(\delta_s, \dot{\psi}) \cos(\psi) + w_y \tag{4}$$

where x and y are the inertial coordinates in the local tangent north–east–down plane, ψ is the yaw or heading angle, $GR(\delta_s, \dot{\psi})$ is the glide ratio, and w_x and w_y are the wind velocity components.

The goal of this study is to establish and analyze the dependences of the glide ratio, descent rate, and yaw rate control authority from the reference canopy asymmetry that will yield the greatest controllability and highest glide without requiring modifications to the canopy geometry. Various static line deflections and the effects on the performance of the cross canopy are quantified, as well as the corresponding controllability concerns (particularly for scenarios with $\delta_s > 0$).

III. Cruciform Parachute Test Article Design

Three initial geometry configurations with varying aspect ratios were developed by the NSRDEC and evaluated in a small-scale wind tunnel at the University of Missouri–Kansas City. Wind-tunnel testing coupled with experience with currently fielded cruciform canopies yielded a reasonable larger-scale canopy configuration for

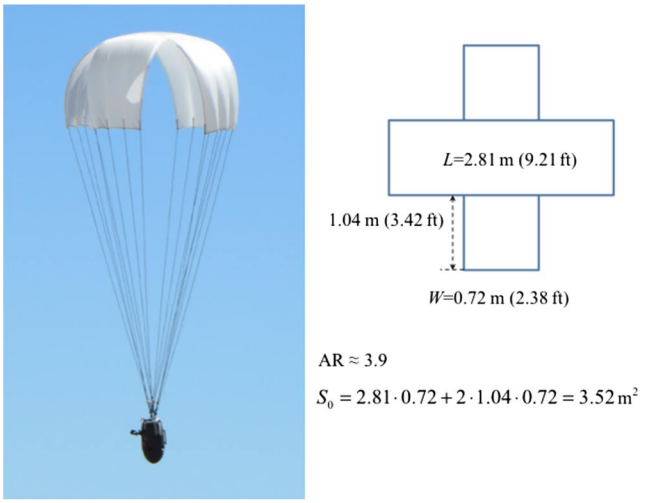

Fig. 6 Geometry of a subscale cruciform canopy.

outdoor drop testing. The dimensions of the identified cross canopy used in this study is shown in Fig. 6.

The autonomous guidance unit (AGU) was created using off-the-shelf electrical hardware and custom-machined aluminum components. The AGU was designed to fit into a 0.2 m (8 in.) diameter, 0.4 m (16 in.) tall pod (Fig. 7a) with a nominal total system weight of 4.65 kg (10.25 lb). The AGU by itself, without bagged canopy and rigging lines (Fig. 7b), has a weight of 4.1 kg (9.5 lb). The system has an operational time of approximately 2 h with a 7.4 V, 2 Ah lithium polymer battery (the actual operational time depends upon the amount of actuation required).

Four groups of suspension lines are rigged to a swivel mechanism developed by the NSRDEC as shown in Fig. 7b. The control line goes through this swivel and is attached to the servoactuator (VSD-11YMB by Vigor Precision) as shown in Fig. 8. The goal of this swivel is to decouple the yaw motion of the canopy from the yaw motion of the pod. As described by Slegers, it is imperative to have either a nearly rigid connection between the payload and parachute or a fully decoupled yaw rotation [28]. If the system is only loosely coupled, then the twisting motion may induce large oscillations, resulting in an unstable and difficult-to-control delivery vehicle.

Other AGU hardware, also shown in Fig. 8, include a microcontroller (X-Monkey by Ryan Mechatronics), an adjustable output voltage regulator (CC BEC Pro by Castle Creations), and high-power RF modem (9XTend by Digi International).

All calculations and actuator control are performed on the highly capable microcontroller. The X-Monkey platform contains an ARM Cortex processor, a Global Positioning System (GPS; ± 2.0 m), a rate gyroscope (± 1.0 deg/s), an accelerometer (± 0.2 m/s^2), a magnetometer (± 0.5 mG), a barometric pressure transducer, six servo

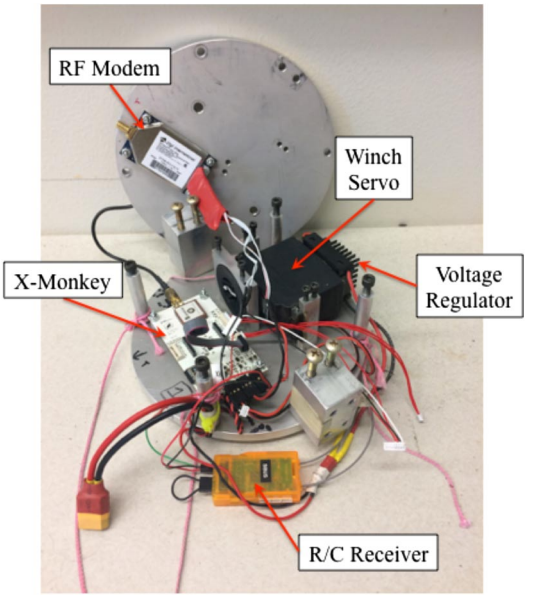

Fig. 8 Single-actuator canopy autonomous guidance unit (R/C, remote control; MSL, mean sea level; ISA, international standard atmosphere).

outputs, micro-secure-digital card logging, two user serial ports, and several general-purpose input/output pins. The attitude estimation algorithm has an estimation uncertainty of ± 1.0 deg, and the GPS-based velocity estimates have a manufacturer reported accuracy of ± 0.1 m/s. Programming is performed in C, where the software framework is provided by the microcontroller manufacturer. The framework software performs all sensor interfacing, output command control, and attitude estimation. Therefore, the user simply needs to develop his/her control code and integrate with the internally available attitude and sensor variables, thereby greatly reducing software development time over fully custom systems. For this study, all data recording and control calculations were conducted at 10 Hz.

IV. Flight-Test Setup

All test operations were conducted at Camp Roberts in California with the use of an Arcturus T-20 unmanned aircraft within the Camp Roberts restricted airspace R-2504 adopted for unmanned aircraft operations. The airspace has an operational ceiling limit of 4.3 km (14,100 ft) above ground level (AGL); however, flights described within this study were limited to 1.1 km (2000 ft) AGL. The catapult-launched T-20 aircraft (Fig. 9a) has a payload capacity of 45 kg (100 lb) and endurance of approximately 10 h (with full payload), and it is autonomously controlled for all aspects of the flight operation from takeoff to landing. On each wing, there is a servoactuated release mechanism specifically designed for aerial and munitions

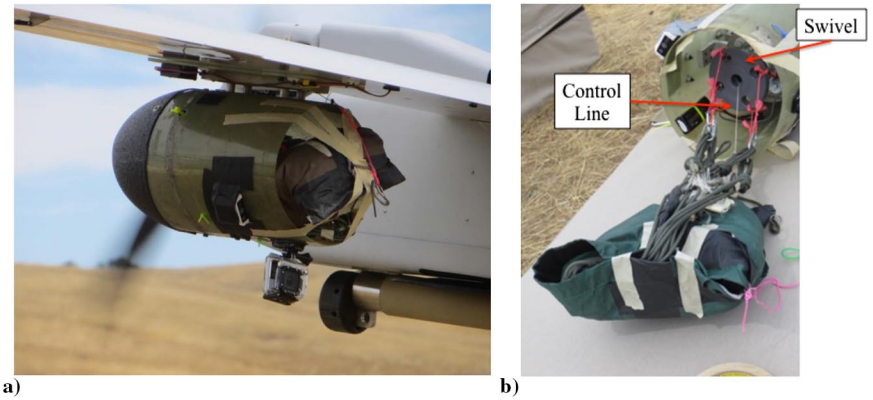

a) b)

Fig. 7 Photographs of a) fully rigged system under the wing of the T-20 UAV, and b) AGU inside the pod attached to a rigged parachute.

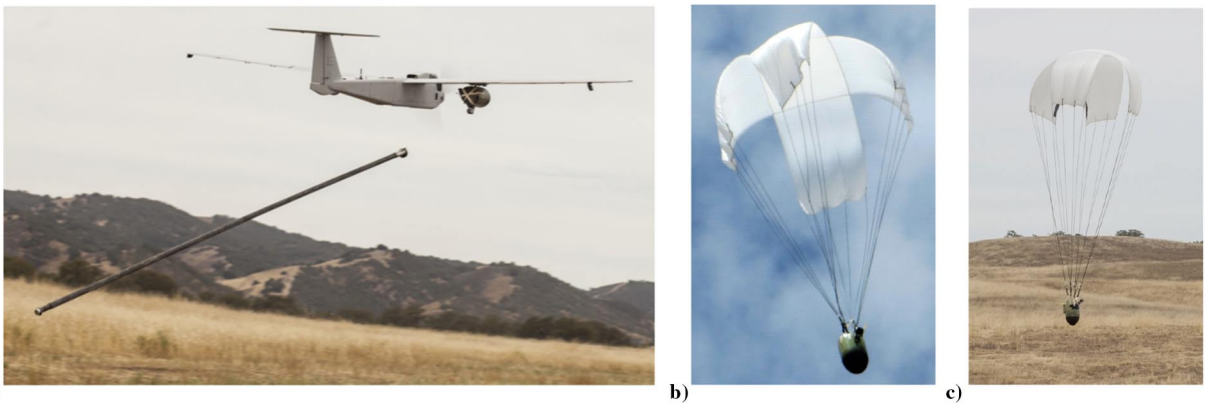

Fig. 9 Photographs of a) Arcturus T-20 UAV carrying two cruciform canopy payloads during launch; and b) fully inflated cruciform canopy in spin mode and c) before touchdown.

delivery, creating an ideal platform for parachute testing operations. Typical aircraft deployment conditions were aircraft speed = 18 m/s (40 mph), deployment altitude = 630 m (2100 ft) AGL, and wind speeds below 5 m/s (11 mph). During dual deployments, the payloads were deployed approximately 1–2 s apart to mitigate the risk of canopy collisions. The parachute was deployed via an approximately 1 m (3.1 ft) static line where the bag remained attached to the T-20 aircraft for the entirety of the flight. Control was triggered immediately after deployment, and the canopy typically reached the wind speed in less than 2 s. In total, 122 individual payload deployments were conducted, with approximately 45 drops conducted with manual control provided by ground personnel to investigate the preliminary capabilities of the system. Additionally, on several drops, the embedded microcontroller failed to record the flight data or the data were corrupted upon retrieval. Finally, the majority of deployments was conducted with the suspension line swivel mechanism. The mechanism inhibits glide ratio estimation, thereby dramatically reducing the effectiveness of the flight-testing effort.

Figure 9b features an example of a spinning canopy [in this particular case, $\delta_s = 11.4$ cm (4.5 in.) and $\delta_c = 0$]. Because it is difficult to visually distinguish the corners attached to the left and right suspension lines, the corresponding canopy edges were painted black. Figure 9c depicts the canopy system during a gliding segment before touchdown.

V. Model Identification

To date, over 100 controlled and simultaneous controlled/uncontrolled airdrops have been executed. Controlled airdrops were intended to investigate the achievable turn rates and tune the yaw angle control system. Controlled airdrops were specifically used to quantify the asymmetric deformation coefficient $k(\delta_s)$, described by Eq. (1), and quantify the effect of yaw rate on the descent rate: $V_d(\delta_s, \dot{\psi})$. Simultaneous airdrops of a controlled and uncontrolled system were used to estimate the achievable glide ratio: $GR(\delta_s, \dot{\psi})$. Specifically, the uncontrolled system was the descent rate matched to the controlled system, thereby providing a zero-glide profile for comparison with the gliding vehicle. The following sections describe these efforts in detail.

A. Turn Rate Dynamics

The turn rate controllability of the cruciform canopy system was quantified through increasing amplitude step response inputs on the single actuator δ_c while keeping δ_s constant. Multiple airdrops were conducted to obtain a statistically verified dependence of the static and control line deflections on the yaw rate: $\dot{\psi} = f(\delta_c, \delta_s)$. The static line deflection was also varied (between flight tests) with both shorter ($\delta_s < 0$) and longer ($\delta_s > 0$) line lengths as compared to the nominal suspension line length.

Figure 10 shows an example of the step inputs profile for a single drop and the corresponding yaw rate responses. This particular drop featured $\delta_s = -11.4$ cm (4.5 in.), which constitutes a 4% shortening

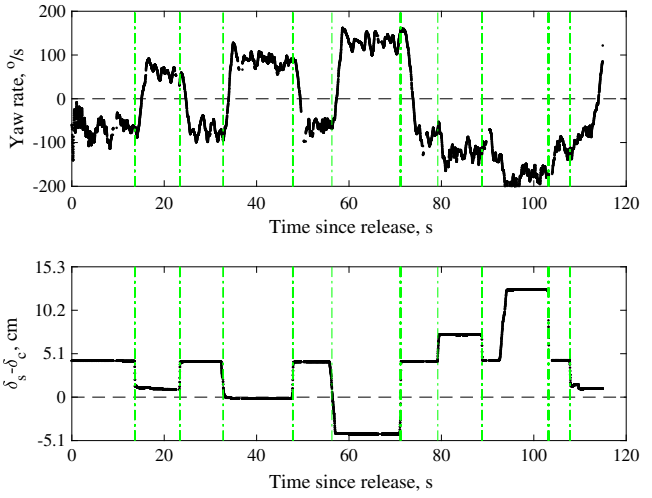

Fig. 10 Step inputs (bottom) and corresponding yaw rate responses (top) with $\delta_s = -11.4$ cm (4.5 in.).

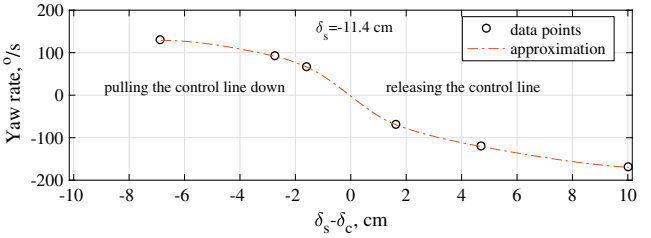

Fig. 11 Yaw rate versus control line deflection with $\delta_s = -11.4$ cm (4.5 in.).

of a suspension line or 15% of canopy arm width W. The relationship between the yaw rate and the control line deflection is nonlinear. As the control line length is shortened, the yaw rate does not proportionally increase. This is likely due to aerodynamic damping of the large canopy coupled with apparent inertia effects from the large volume of air within the canopy. The nonlinearity can be more clearly seen in Fig. 11, which presents an experimentally derived correlation between the yaw rate and the control line deflection ($\dot{\psi} = f(\delta_c, \delta_s) = -11.4$ cm) derived from the data of Fig. 10. The model approximation has a cubic shape, indicating reduced control line deflection effectiveness at the extreme deflections. Interestingly, the data indicate a nearly symmetric yaw rate effectiveness for shortened and extended control line deflections. However, flight testing reveals the canopy has excessive panel flapping with large positive deflections, which is likely due to the limited loading on the extended suspension line. Another important aspect that can be

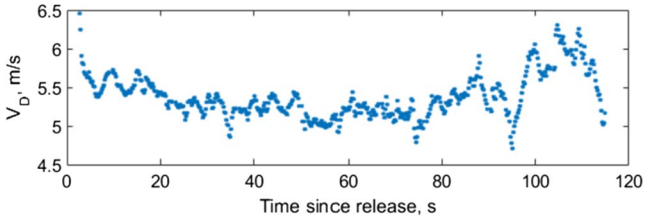

Fig. 12 Descent rate profile for the airdrop shown in Fig. 10.

identified from the flight-test data is the dependency of the yaw rate and static line deflection on the descent speed. For a representative flight test, Fig. 12 provides the descent speed. No explicit effect of the turn rate on the descent rate can be identified, thereby indicating that the descent speed is approximately constant, regardless of the control input: $V_d(\dot{\psi}, \delta_s) = -11.4$ cm = const. Additional flight testing needs to be conducted to ensure the relationship holds for other static line deflections. A potential explanation for the negligible effect on the descent speed is the possible lift generation from the spinning canopy. As the parachute reduces the drag area, the yaw rate increases, thereby increasing the spinning-generated lift. The ability to neglect yaw rate effects on the descent speed has profound implications on the precision guidance strategy, particularly because the coupling between the glide and descent speed is eliminated, greatly reducing the complexity associated with a coupled dynamic model. The sensor-based attitude and actuation estimate uncertainties are sufficiently low to have minimal effect on the model estimation when compared with the larger disturbances introduced by the highly flexible canopy.

An analysis of data for this series of drops also included identification of the turn rate dynamics as a function of the static and control line deflections. Specifically, a linear model [Eq. (1)] and a second-order model were examined. It was determined that the second-order response yields a better match of the system behavior for all δ_s configurations tested. Figure 13 shows the response of an estimated second-order model and an actual system to the step input. The test data shown are the same data used to generate Figs. 10–12. The turn dynamics were estimated using the MATLAB System Identification Toolbox. The yaw rate and input command were used to generate the transfer function model. To facilitate more realistic results, a discrete transfer function formulation was estimated. The discrete model was set to second order with no zeros. Negligible improvement in the model fit was accomplished with a higher-order model or with the addition of zeros. Although the model does not capture all of the actual motion, it does provide a good estimate of the turn rate dynamics. Some of the disparities between the model and experimental results are caused by the relative rotation between the payload and canopy (from the installed swivel mechanism). Additionally, the yaw rate bias introduced with nonperfect trim conditions hindered the model estimation results. Therefore, the model estimates the trend of the negative yaw rate motion but cannot adequately overcome the large negative bias:

$$H(z) = \frac{1.141e^{-6}}{1 - 1.988z^{-1} + 0.9886z^{-2}} \tag{5}$$

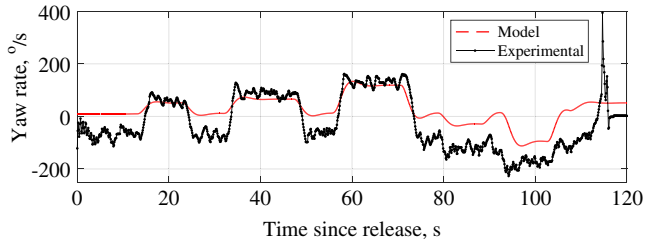

Fig. 13 Yaw rate response for the actual system without a swivel versus its model.

The limitations invoked by the swivel mechanism warrant additional discussion. The swivel was originally installed to prevent wrapping of the control line with the remaining suspension lines. During descent, the payload would deflect the control line, causing the parachute to begin rotating. In a relatively short amount of time (typically less than 1 s for high rate maneuvers), the payload would approach a zero-relative rotation scenario. Essentially, the swivel acts to filter high-frequency canopy motion from acting on the payload. Therefore, only the steady-state rate values were taken from testing with a swivel. All model identification results were computed from testing without the swivel installed. Attempting to evaluate gliding performance is not possible with the swivel installed, as the parachute is often pointing in a different direction when compared to the payload and it varies during the descent. The result is the payload attempting to point in a particular direction, but the canopy may not be pointing in the same direction (as the swivel has rotated the canopy to a different orientation). By removing the swivel, the gliding capability can be investigated. For all glide ratio estimation, only results without the swivel mechanism are included.

B. Glide Ratio Capability

To determine the achievable glide ratio while varying δ_s, two problems need to be addressed. First, the system needs to be stabilized with $\psi^{\&} \approx 0$ (there is no glide while the system is spinning). Second, wind data need to be available to remove the translational effects induced by the atmospheric winds. Determining a glide ratio is accomplished by resolving Eqs. (3) and (4) as

$$GR(\delta_s, \dot{\psi} = 0) = \frac{\sqrt{(\dot{x} - w_x)^2 + (\dot{y} - w_y)^2}}{\dot{z}} \tag{6}$$

(here, we assume $w_z \approx 0$.)

A proportional-integral-derivative (PID) controller [Eq. (7)] was developed to enable yaw rate control. For all glide ratio testing, the desired yaw rate ψ_{des} was set to zero:

$$\delta_c = (K_P + K_I s^{-1} + K_D s)(\dot{\psi} - \dot{\psi}_{\text{des}}) \tag{7}$$

The PID controller was developed and tuned using the turn rate step response data [Eq. (5)] with the MATLAB Control System Toolbox. The gains of the PID controller [Eq. (6)] were identified as $K_P = 440$, $K_I = 140$, and $K_D = 4.4$. Figure 14 shows an example of zeroing the yaw rate during one of the flight tests.

Quantification of the canopy glide ratio requires the determination of the wind components during descent, which would ideally require launching a balloon or deploying a dropsonde immediately before the canopy descent. However, due to limited resources, an alternative approach was used. Two nearly identical cruciform parachute systems were deployed with one of them (referred to as the uncontrolled system) allowed to inflate normally (zero line deflections) and a controlled cruciform parachute system with the developed rate controller, which attempts to zero the yaw rate after a full deployment of a canopy. Assuming that the uncontrolled system exhibits no glide, Eq. (6) can be rewritten as

$$GR(\delta_s, \dot{\psi} = 0) = \frac{\sqrt{(\dot{x}_{\text{con}} - \dot{x}_{\text{unc}})^2 + (\dot{y}_{\text{con}} - \dot{y}_{\text{unc}})^2}}{\dot{z}_{\text{con}}} \tag{8}$$

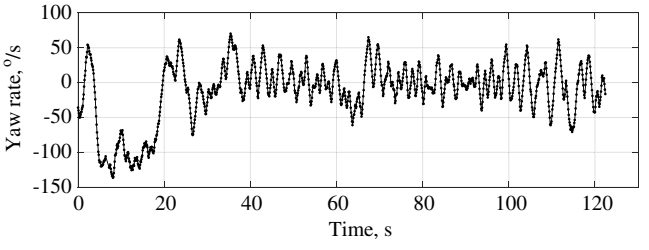

Fig. 14 Zeroing the yaw rate with a PID controller.

Fig. 15 Simultaneously deployed controlled (on the left) and uncontrolled (on the right) parachutes.

i.e., the deviation between the two systems is considered as a direct result of the glide achieved by the controlled system. An example of such a simultaneous controlled/uncontrolled airdrop is shown in Fig. 15 (looking at the colored edges of the controlled system, it can be observed that the controlled system deviates to the left, i.e., away from the uncontrolled system), whereas Fig. 16 features a bird's-eye view of this airdrop. The inconsistent separation of the two payloads is likely caused by the inaccuracy in the heading control algorithm to maintain a zero yaw rate during descent. However, the contributions of each time step on the glide can be accumulated to generate a maximum theoretical glide ratio in addition to the conservative glide ratio achieved by examining the separation distance upon landing.

Figure 17 shows the changing ground speed magnitude of both systems and the difference between them caused primarily by the glide capability of the controlled system. When applying Eq. (8), all quantities were used at the same altitude, which required using the interpolation of data for the uncontrolled system based on the descent rate profile (also shown in Fig. 17). Although difficult to see, the difference in horizontal speed between the uncontrolled and controlled payloads is shown with the dashed line in the left graph. The average difference in ground speeds V_G is the horizontal speed between the two systems is $V_h = 1.3$ m/s, which can then be used to estimate the average glide ratio of $GR = 0.25$ when using the average descent speed. This result is significant because the estimate is conservative in the highest achievable glide ratio estimate. This is because the system does not maintain the desired heading perfectly, and any control actuations will reduce the gliding effectiveness through both suboptimal control line deflections and gliding in an oscillatory path rather than a direct path.

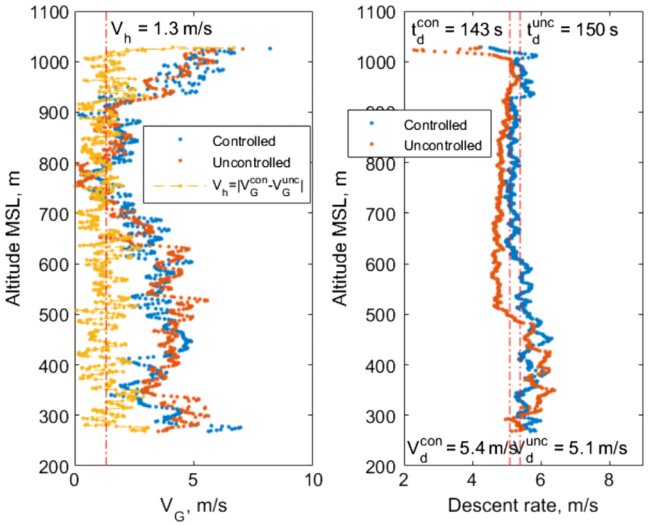

Fig. 17 Ground speed (left) and descent rate (right).

A vertical profile for a computed value of the GR at each time step during descent is presented in Fig. 18. This figure also features computed profiles of the air density for both systems based on recordings of air pressure and air temperature. Here, the maximum glide ratios of 0.5 are achieved, indicating potentially significant gliding performance with a more accurate heading control system. The maximum glide ratios of 0.5 correlate well with the previous testing effort completed by Potvin et al. [21]. An air density profile of the standard international atmosphere model, also shown in Fig. 18, indicates that those operations were conducted during a very hot day with a high-density altitude.

As a byproduct of the glide ratio estimation, an aerodynamic drag coefficient was estimated for both controlled and uncontrolled cruciform parachute systems using the standard quadratic drag model formulation:

$$C_D = \frac{2\,m(g - a_z)}{\rho V_d^2 S_0} \approx \frac{2\,mg}{\rho V_d^2 S_0} \tag{9}$$

For the drop test depicted in Figs. 17 and 18, the drag coefficients throughout the descent for the controlled and uncontrolled systems are shown in Fig. 19. As expected, the nearly identical payloads exhibit similar drag characteristics, and no discernible difference is seen even when the controlled parachute is deflected during descent. Additionally, the results correlate well with the reported drag coefficient range of

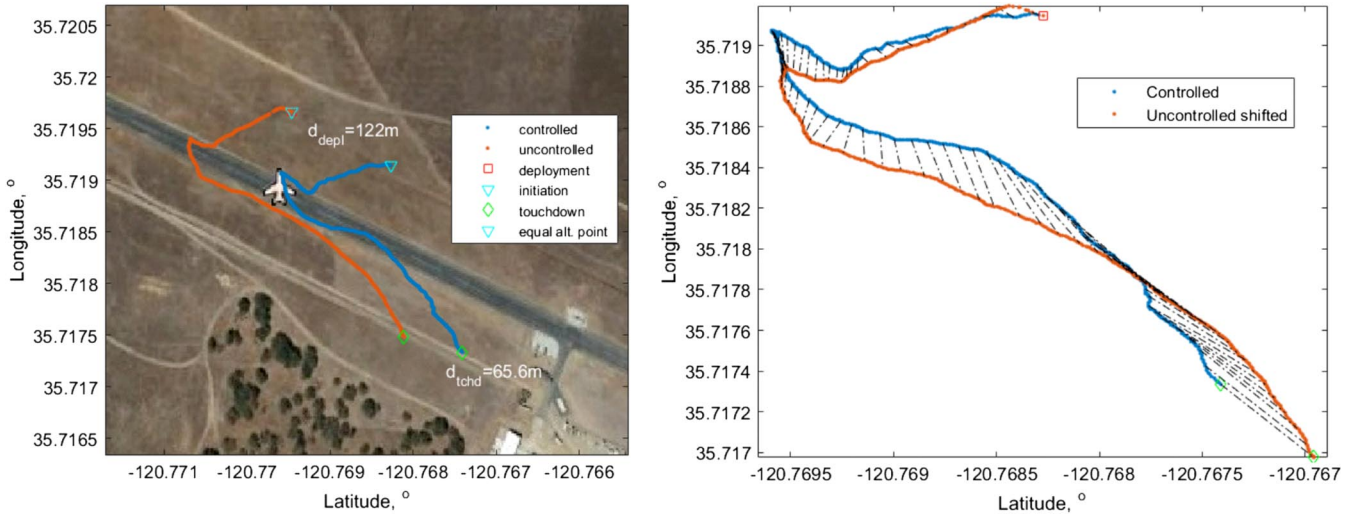

Fig. 16 Bird's-eye view of a double airdrop (left), and the difference between two trajectories (shifted to originate at the same point) (right).

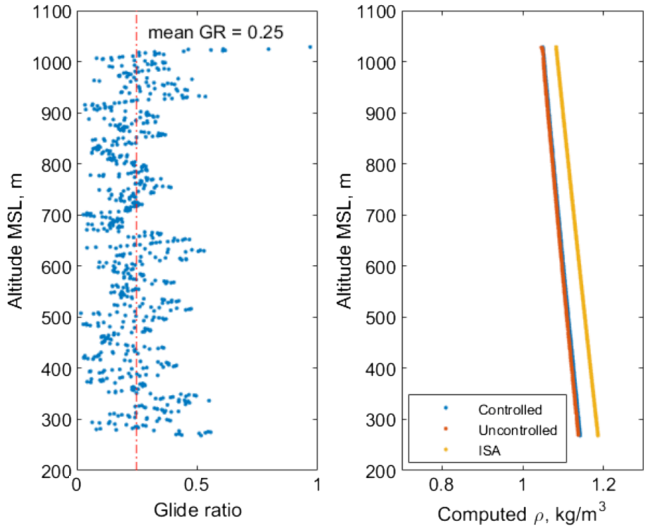

Fig. 18 Glide ratio and computed air density versus altitude MSL.

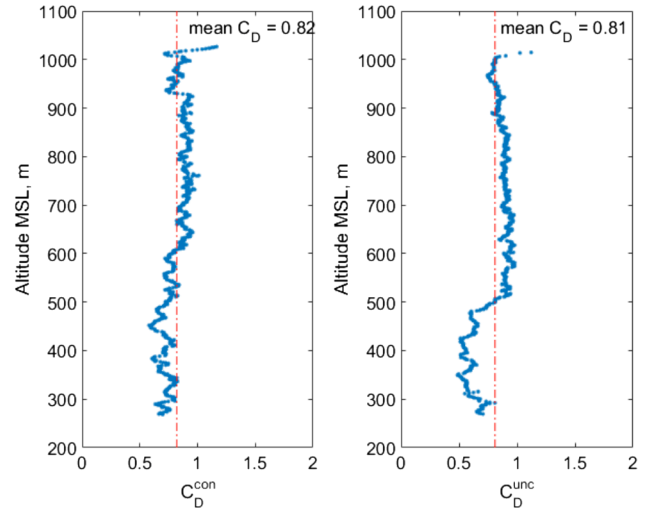

Fig. 19 Aerodynamic drag coefficients for controlled (left) an uncontrolled (right) systems.

0.60–0.85 for cross canopies reported in the *Parachute Recovery Systems Design Manual* [29].

Table 1 consolidates the glide ratio values and other data obtained for two different δ_s configurations, and Fig. 20 represents the glide ratio versus δ_s results graphically. Although over 100 drops have been performed, only a small percentage were simultaneous deployments with fully successful hardware and software (i.e., working heading controller, no swivel, and successful parachute deployments). Additionally, other static line deflections were evaluated; however, the swivel was still attached, thereby inducing large uncertainties into the glide estimation.

Table 1 Estimated parameters for two asymmetry configurations δ_s

δ_s, cm	V_h, m/s	V_d^{con}/V_d^{unc}, m/s	GR	C_D^{con}/C_D^{unc}
−11.4	1.3	5.4/5.1	0.25	0.82/0.81
−11.4	1.6	6.4/5.6	0.25	0.61/0.66
−11.4	1.5	6.4/5.8	0.23	0.59/0.64
−11.4	2.0	6.0/6.0	0.34	0.68/0.67
−11.4	3.0	4.1/4.6	0.74	1.3/1.0
−16.5	1.8	5.3/4.8	0.34	0.85/0.96

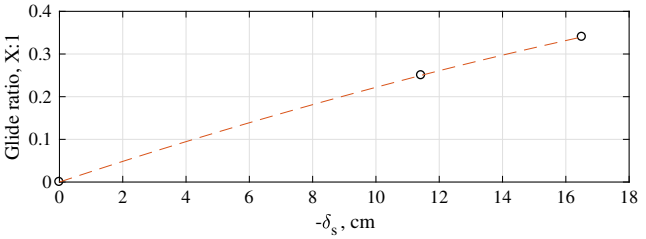

Fig. 20 Glide ratio versus δ_s configuration.

Qualitatively, testing scenarios with positive static line deflections (longer line than the nominal suspension line) were inadequate for precision aerial delivery. The primary concerns were the stability and repeatability of the canopy, as the canopy panels tended to flap freely during descent.

The results provided in Table 1 indicate an average glide of 0.27 for $\delta_s = -11.4$ cm (0.37 ft) when neglecting the unreasonably large glide ratio of 0.74. The high glide is likely due to thermal activity, as indicated by the very high drag coefficients for the two systems. Although there are not sufficient data to be statistically confident in the results, it appears as though the higher static line deflection of $\delta_s = -16.5$ cm (0.54 ft) provides a higher glide ratio. When comparing the drag coefficients of the first and last flight tests in Table 1, the coefficients are approximately equal, indicating similar descent performance of the canopies. Therefore, from this feasibility study, a static line deflection of $\delta_s = -16.5$ cm, or approximately 6% of the original suspension line length, is recommended to yield greater horizontal glide. Higher deflections were tested, but the canopy was prone to skirt inversion and canopy collapse during descent.

VI. Conclusions

This paper describes the development and evaluation of a single actuator-based cross-canopy autonomous decelerator vehicle. A small-scale vehicle was created to increase the efficiency of data collection efforts through the use of unmanned–aerial-vehicle-based canopy deployment operations. In total, 122 payload deployments have been conducted, providing relevant data for the quantification of the yaw rate controllability and the glide ratio capability of the cross-canopy vehicle. It is important to note that many payload deployments were conducted with the attached swivel mechanism, thereby dramatically limiting the quantification of accurate glide ratio information. Yaw rate control testing indicated greater actuator-driven response with a shortened static line, and it resulted in a negligible increase in payload descent speed. Although difficult to measure, the glide ratio ranged from approximately 0.23 to 0.34, indicating some lateral control capability. The developed autonomous descent vehicle has been shown to be a feasible delivery system, requiring an inexpensive canopy design and only a single actuator for yaw and lateral control. For increased effectiveness, the suspension lines should be anchored directly to the payload to limit relative rotation and the yaw angle control system should have the best possible accuracy to realize the greatest glide capabilities of the canopy. The system has the potential to increase precision delivery capabilities, particularly when the system cost inhibits parafoil-based deliveries, and it enables pure vertical (relative to wind) descent profiles that are not currently achievable with high-glide systems.

Acknowledgments

The authors would like to thank the U.S. Army Natick Soldier Research Development and Engineering Center (NSRDEC) and the Consortium for Robotics and Unmanned Systems Education and Research at the Naval Postgraduate School for the financial support of the research. Additionally, they would also like to thank Arcturus UAV for providing the air-lift operations. The authors would like to acknowledge and thank Richard Benney of the NSRDEC for the original concept and technical discussions for the steerable cruciform canopy. The NSRDEC is in the process of patenting the steerable concept and many other low-cost low-glide airdrop capabilities, and several airdrop systems are currently being analyzed for feasibility

and cost effectiveness for further development. The authors would like to thank Daniel Nyren of the NSRDEC for the initial canopy geometries and the swivel system.

References

[1] Yakimenko, O., (ed.), *Precision Aerial Delivery Systems: Modeling, Dynamics, and Control*, Progress in Astronautics and Aeronautics, AIAA, Reston, VA, 2015, pp. 391–528.

[2] Benney, R., Barber, J., McGrath, J., McHugh, J., Noetscher, G., and Tavan, S., "The Joint Precision Airdrop System Advanced Concept Technology Demonstration," *18th AIAA Aerodynamic Decelerator Systems Technology Conference and Seminar*, AIAA Paper 2005-1601, 2005.

[3] Slegers, N., and Costello, M., "Aspects of Control for a Parafoil and Payload System," *Journal of Guidance, Control, and Dynamics*, Vol. 26, No. 6, 2003, pp. 898–905. doi:10.2514/2.6933

[4] Yakimenko, O., "On the Development of a Scalable 8-DoF Model for a Generic Parafoil-Payload Delivery System," *18th AIAA Aerodynamic Decelerator Systems Technology Conference and Seminar*, AIAA Paper 2005-1665, 2005.

[5] Yakimenko, O., "Development and Testing of the Miniature Aerial Delivery System Snowflake," *20th AIAA Aerodynamic Decelerator Systems Technology Conference and Seminar*, AIAA Paper 2009-2980, 2009.

[6] Slegers, N., Beyer, E., and Costello, M., "Use of Variable Incidence Angle for Glide Slope Control of Autonomous Parafoils," *Journal of Guidance, Control, and Dynamics*, Vol. 31, No. 3, 2008, pp. 585–596. doi:10.2514/1.32099

[7] Bergeron, K., Fejzic, A., and Tavan, S., "Accuglide 100: Precision Airdrop Guidance and Control via Glide Slope Control," *21st AIAA Aerodynamic Decelerator System Technology Conference and Seminar*, AIAA Paper 2011-2530, 2011. doi:10.2514/6.2011-2530

[8] Scheuermann, E., Ward, M., Cacan, M., and Costello, M., "Combined Lateral and Longitudinal Control of Parafoils Using Upper-Surface Canopy Spoilers," *Journal of Guidance, Control, and Dynamics*, Vol. 38, No. 11, 2015, pp. 2122–2131. doi:10.2514/1.G000892

[9] Fields, T. D., LaCombe, J. C., and Wang, E. L., "Autonomous Guidance of a Circular Parachute Using Descent Rate Control," *Journal of Guidance, Control, and Dynamics*, Vol. 35, No. 4, 2012, pp. 1367–1370. doi:10.2514/1.55919

[10] Fields, T. D., LaCombe, J. C., and Wang, E. L., "Time Varying Descent Rate Control Strategy for Circular Parachutes," *Journal of Guidance, Control, and Dynamics*, Vol. 38, No. 8, 2015, pp. 1468–1477. doi:10.2514/1.G000627

[11] Fields, T. D., LaCombe, J. C., and Wang, E. L., "Flight Testing of a 1-DOF Variable Drag Autonomous Descent Vehicle," *22nd AIAA Aerodynamic Decelerator Systems Technology Conference and Seminar*, AIAA Paper 2013-1377, 2013.

[12] Fields, T. D., "Evaluation of Control Line Reefing Systems for Circular Parachutes," *Journal of Aircraft*, Vol. 53, No. 3, 2016, pp. 855–860. doi:10.2514/1.C033524

[13] Brown, G., Haggard, R., Almassy, R., Benney, R., and Dellicker, S., "The Affordable Guided Airdrop System (AGAS)," *15th AIAA Aerodynamic Decelerator Systems Technology Conference and Seminar*, AIAA Paper 1999-1742, 1999.

[14] Dellicker, S. H., and Bybee, J., "Low Cost Parachute Guidance, Navigation, and Control," *15th AIAA Aerodynamic Decelerator Systems Conference*, AIAA Paper 1999-1706, 1999.

[15] Yakimenko, O. A., Dobrokhodov, V. N., and Kaminer, I. I., "Synthesis of Optimal Control and Flight Testing of an Autonomous Circular Parachute," *Journal of Guidance, Control, and Dynamics*, Vol. 27, No. 1, 2004, pp. 29–40. doi:10.2514/1.9282

[16] Gilles, B., Hickey, M., and Krainski, W., "Flight Testing of a Low-Cost Precision Aerial Delivery System," *18th AIAA Aerodynamic Decelerator Systems Technology Conference and Seminar*, AIAA Paper 2005-1651, 2005.

[17] Jorgensen, D. S., and Hickey, M. P., "The AGAS 2000 Precision Airdrop System," *Infotech@Aerospace*, AIAA Paper 2005-7072, 2005.

[18] LaFarge, R. A., Nelsen, J. M., and Gwinn, K. W., "A Novel CFD/Structural Analysis of a Cross Parachute," *32nd AIAA Aerospace Sciences Meeting and Exhibit*, AIAA Paper 1994-752, 1994.

[19] Levin, D., and Shpund, Z., "Canopy Geometry Effect on the Aerodynamic Behavior of Cross-Type Parachutes," *Journal of Aircraft*, Vol. 34, No. 5, 1997, pp. 648–652. doi:10.2514/2.2224

[20] Shpund, Z., and Levin, D., "Dynamic Investigation of Asymmetric Cross-Type Parachutes," *14th AIAA Aerodynamic Decelerator Systems Technology Conference and Seminar*, AIAA Paper 1997-1526, 1997.

[21] Potvin, J., Papke, J., Brighton, E., Hawthorne, T., Peek, G., and Benney, R., "Glide Performance Study of Standard and Hybrid Cruciform Parachutes," *17th AIAA Aerodynamic Decelerator Systems Technology Conference and Seminar*, AIAA Paper 2003-2160, 2003.

[22] Forichon, A., "Parachute," U.S. Patent 2,997,263, 1961.

[23] Nice, R. J., Haak, E. L., and Guteneauf, R., "Drag and Stability of Cross-Type Parachutes," Univ. of Minnesota, Rept. FDL-TDR-64-155, Minneapolis, MN, 1965.

[24] Ludtke, W., "Effects of Canopy Geometry on the Spinning Characteristics of a Cross Parachute with a W/L RATIO of 0.264," Naval Ordnance Lab., NOLTR 71-111, White Oak, Silver Springs, MD, Aug. 1971.

[25] Jorgensen, D. S., "Cruciform Parachute Aerodynamics," Ph.D. Dissertation, Univ. of Leicester, Leicester, England, U.K., 1982.

[26] Shen, C. O., and Cockrell, D. J., "Aerodynamic Characteristics and Flow Round Cross Parachutes in Steady Motion," *Journal of Aircraft*, Vol. 25, No. 4, 1988, pp. 317–323. doi:10.2514/3.45566

[27] Han, Y. H., Wang, Y. W., Yang, C. X., and Xiao, J., "Numerical Methods for Analyzing the Aerodynamic Characteristics of Cross Parachute with Permeability," *22nd AIAA Aerodynamic Decelerator Systems Technology Conference*, AIAA Paper 2013-1283, 2013.

[28] Slegers, N. J., "Comparison of Parafoil Dynamic Modes with Varying Payload Connections," *24th AIAA Aerodynamic Decelerator Systems Technology Conference*, AIAA Paper 2017-3878, 2017.

[29] Knacke, T., *Parachute Recovery Systems Design Manual*, 1st ed., Para Publishing, Santa Barbara, CA, 1992, p. 5-3.